Vibrational dynamics of a two-dimensional microgranular crystal

A. Vega-Flick, R. A. Duncan, S. P. Wallen, N. Boechler, C. Stelling, M. Retsch, J. J. Alvarado-Gil, K. A. Nelson, and A. A. Maznev

Phys. Rev. B **96**, 024303 — Published 24 July 2017

DOI: 10.1103/PhysRevB.96.024303

Vibrational dynamics of a two-dimensional micro-granular crystal

A.Vega-Flick,[1,2,*] R. A. Duncan,[1] S. P. Wallen,[3] N. Boechler,[3] C. Stelling,[4]
M. Retsch,[4] J.J. Alvarado-Gil,[2] K. A. Nelson,[1] and A. A. Maznev[1,•]

[1] *Department of Chemistry, Massachusetts Institute of Technology, Cambridge, Massachusetts 02139, USA*
[2] *Applied Physics Department, CINVESTAV-Unidad Mérida, Carretera Antigua a Progreso Km 6, Cordemex, Mérida, Yucatán, 97310, México*
[3] *Department of Mechanical Engineering, University of Washington, Seattle, WA, 98195 USA*
[4] *Physical Chemistry, University of Bayreuth, Universitaetsstr 30, 95447 Bayreuth, Germany*

We study the dynamics of an ordered hexagonal monolayer of polystyrene microspheres adhered to a glass substrate coated with a thin aluminum layer. A laser-induced transient grating technique is employed to generate and detect three types of acoustic modes across the entire Brillouin zone in the Γ-K direction: low-frequency contact-based modes of the granular monolayer, high-frequency modes originating from spheroidal vibrations of the microspheres, and surface Rayleigh waves. The dispersion relation of contact-based and spheroidal modes indicates that they are collective modes of the microgranular crystal controlled by particle-particle contacts. We observe a spheroidal resonance splitting caused by the symmetry breaking due to the substrate, as well as an avoided crossing between the Rayleigh and spheroidal modes. The measurements are found to be in agreement with our analytical model.

I. INTRODUCTION

Vibrations of periodic arrays of spheres interacting via Hertzian contacts initially attracted attention following the discovery of solitary wave propagation in the "sonic vacuum" regime of a 1D chain of uncompressed spheres[1,2]. Subsequent studies were extended to 2D and 3D systems and yielded an array of novel acoustic phenomena[3]. Granular crystals, as these systems became known, can be considered a class of phononic crystal[4] with unique behavior specific to granular media. For instance, in addition to nonlinear effects such as solitons and discrete breathers[2,3], unusual linear phenomena such as the existence of rotational acoustic modes have been revealed[5,6]. Due to the nonlinearity of Hertzian contacts, the acoustic properties of granular crystals can be easily tuned, for example by applying static compression, which makes them attractive for potential applications[3].

Until very recently, granular crystal studies were conducted with macroscopic particles such as ball bearings. A new frontier was opened by laser-based experiments on 2D self-assembled monolayers of micron-sized particles on a solid substrate[7–11]. These experiments revealed the crucial role of adhesion, which is negligible for large particles but becomes an important factor in determining the contact stiffness at the microscale. The initial efforts focused on the vertical contact resonance of microspheres, arising due to contact with the substrate, and its interaction with surface acoustic waves (SAWs). In these initial studies, the observed phenomena, such as an avoided crossing in the Rayleigh SAW dispersion[7] and the resonant attenuation of SAWs by microspheres[9], could be well accounted for by a simple model where microspheres did not interact with each other[7]. Refined measurements of the resonant attenuation of SAWs revealed horizontal-rotational modes enabled by interparticle interactions[10]. However, none of the experiments performed on self-assembled microgranular monolayers were done on a "single crystal" sample with long-range order extending over distances comparable to the measurement spot size. The observed phenomena were limited to the regime in which the acoustic wavelength was much greater than the sphere size and the long-range periodic order was not essential. The purpose of this work is to study vibrational properties of a well-ordered "single crystal" lattice of microspheres, i.e., a true 2D microscale granular crystal.

An analogy can be drawn between a 2D granular crystal and a 2D lattice of atoms such as graphene. However, there is an important difference, as vibrations of a granular monolayer involve rotations of the spheres[10,12]. Spheres also have internal mechanical degrees of freedom; consequently, in addition to contact-based modes, one would expect to see collective modes originating from spheroidal vibrations of the spheres[13]. The presence of the substrate significantly alters the dispersion of contact-based modes[14] and adds Rayleigh SAWs in the substrate, which interact with the vibrational modes of the monolayer[10,14]. In this work, we characterize the dispersion of these three types of modes (contact-based, spheroidal, and Rayleigh) and their interaction across the entire Brillouin zone (BZ) for a chosen high symmetry direction of a 2D microgranular crystal.

II. METHODOLOGY

A. Sample description

Our sample is a 2D monolayer of $1.5 \pm 0.023\,\mu$m diameter polystyrene spheres adhered to a float glass substrate coated with a 100 nm aluminum film. The microspheres are arranged in a highly ordered hexagonal lattice shown in Fig. 1(a). The sample preparation followed the approach described by Retsch et al.[15]. Briefly, a 3 wt% dispersion of particles in ultrapure (MiliQ) water was spin

coated on a cationically functionalized glass slide at a speed of 4000 rpm. The particle-coated substrate was slowly immersed into a 0.1 mM SDS solution in MiliQ water, which was adjusted to pH 12 with aqueous amonium hydroxide solution. The particles were assembled at the air/water interface into a freely floating monolayer, which was finally transferred to an aluminum coated glass substrate and dried in air.

B. Experiment

A laser-induced transient grating technique[16,17] was used to excite and probe acoustic modes of the structure. Two excitation pulses derived from the same laser source (515 nm wavelength, 60 ps pulse duration, 0.6 μJ total energy at the sample, 860 μm spot diameter at $1/e^2$ intensity level) were overlapped at the sample as shown in Fig. 1(b), forming an interference pattern of period λ. Absorption of the laser light by the aluminum film induced rapid thermal expansion, which generated counter-propagating acoustic modes with wavelength λ[17]. The wavelength can be varied by switching the diffraction grating pattern used to produce the excitation beams pair and fine-tuned by tilting it[18]. The detection of acoustic vibrations was accomplished via diffraction of a quasi-cw probe laser beam (532 nm wavelength, 200 μm spot diameter, 160 mW power at the sample) with optical heterodyne detection[19,20]. The optical diffraction pattern from the microspheres was monitored, as shown in Fig. 1(c), to ensure that the laser spot was located in a highly ordered area, and to align the acoustic wave vector along the Γ-K direction of the reciprocal lattice as shown in Fig. 1(d).

Figure 2(a) shows typical signal waveforms measured at three different acoustic wave vectors. The corresponding Fourier spectra shown in Fig. 2(b) reveal the presence of many acoustic modes. By plotting the identified frequencies for each wave vector[21], we obtained the dispersion curves shown in Fig. 2(c). Three different types of acoustic modes can be identified: a mode labeled R with a nearly constant dispersion slope corresponding to the SAW velocity of the substrate; low frequency modes (HR, V, RH) with weaker frequency dependence, which we identify as contact-based modes[14] and high frequency nearly flat branches (S) corresponding to spheroidal vibrational modes of the spheres.

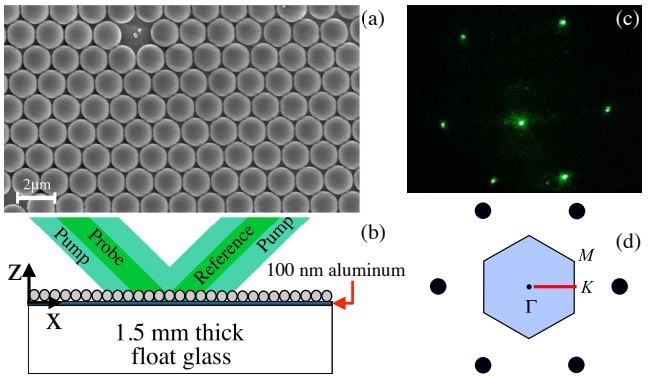

FIG. 1. (a) Scanning electron microscope image of the microsphere monolayer. (b) Schematic of the experiment. (c) Diffraction pattern produced by the probe laser beam in reflection. (d) Reciprocal lattice and the first BZ of the microgranular crystal; red-line shows the wave vector range used in the experiment.

The Rayleigh mode dispersion is "zone-folded" at the BZ boundary (in Fig. 2(b) this zone-folding is seen in the presence of two Rayleigh peaks at $q = 1.7\,\mu\text{m}^{-1}$). The zone-folding of the SAW dispersion at the expected location of the BZ boundary in the Γ-K direction confirms the "single crystal" structure of the sample and the correct orientation of the acoustic wave vector with respect to the microsphere lattice. Otherwise the SAW is virtually unaffected by the microspheres, with the exception of avoided crossings discussed below.

III. CONTACT-BASED MODES

Figure 2(d) presents a more detailed view of the dispersion of low frequency contact-based modes. The mode labeled V corresponding to the most prominent peak in the spectra, as shown in Fig. 2(e), has been previously identified as the vertical contact resonance mode[7,9,10]. Fig. 2(e) also shows small peaks to either side of the V mode peak which we assigned to horizontal-rotational modes labeled HR and RH following Ref.[14]. The avoided crossing between the vertical resonance mode and the SAW, studied in previous works[7,9], is just outside the wave vector range of our measurements. In the absence of inter-particle interactions, the contact resonance frequency, past the avoided crossing with the SAW, is expected to be independent of the wave vector[7]. The interaction between microspheres should result in dispersion, predicted in Ref.[14] but not observed in previous studies due to the lack of long-range order in the samples. As can be seen in Fig. 2(d), our data clearly show the expected dispersion, indicating that we observe a collective mode of the microgranular crystal rather than vibrations of non-interacting particles.

A model describing vibrations of a monolayer of spheres on a substrate accounting for both sphere-substrate and sphere-sphere contacts has been developed for a square lattice[14] and subsequently modified for a hexagonal lattice[22]. The model yields three vibrational modes polarized in the sagittal plane[23]; one of them predominantly involves vertical displacements while the other two have primarily horizontal-rotational character. The diffraction of the probe beam is most sensitive to the vertical mode, which is the most prominent in the data.

The model treats the sphere-substrate and sphere-sphere contacts as normal and shear springs, with spring constants K_N, K_S corresponding to sphere-substrate and

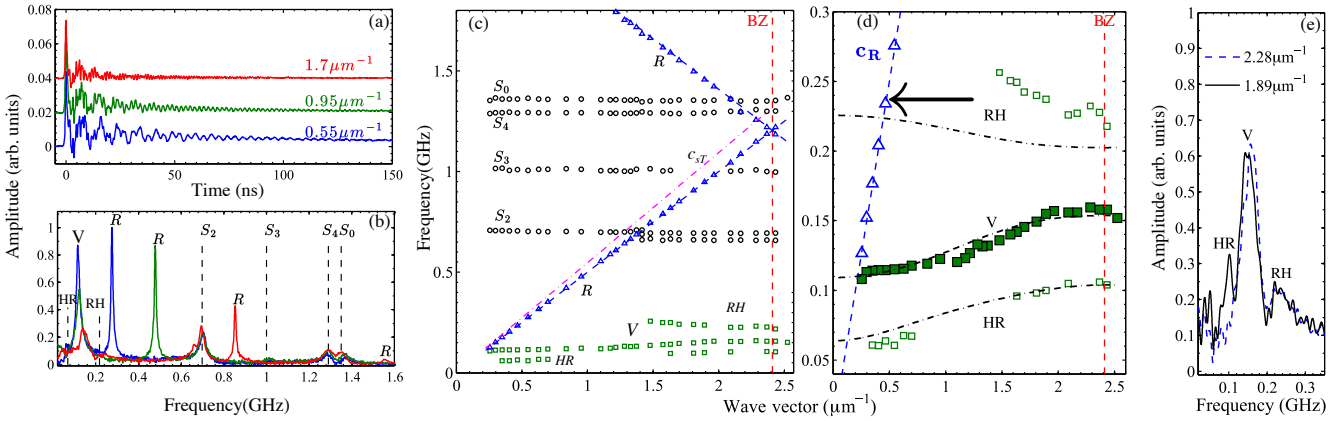

FIG. 2. (a) Signal waveforms for three different wave vectors and (b) corresponding Fourier spectra. Peaks labeled V and R correspond to the vertical contact resonance mode and SAWs, respectively. Spheroidal modes are labeled S_0, S_2, S_3, S_4 according to their angular number L. (c) Measured dispersion of different modes labeled as in (b). Blue dashed line corresponds to SAW velocity for the substrate, red vertical dashed line corresponds to the BZ boundary. The dashed-dotted line corresponds to the transverse velocity of the substrate c_{sT}. (d) Dispersion in the range $0.05 - 0.3$GHz. Solid markers represent the predominantly vertical V mode, smaller hollow markers the horizontal-rotational HR and RH modes. Dashed-dotted lines are theoretical calculations. Horizontal arrow indicates the maximum SAW attenuation. (e) Fourier spectra for two representative wave vectors showing the HR and RH peaks.

G_N, G_S to sphere-sphere contacts, where subscripts N and S refer to normal and shear, respectively. For a Hertz-Mindlin contact[24], the ratio of normal and shear spring constants is determined by the elastic constants of the contacting materials[22]. Thus the model only has two independent parameters, K_N and G_N.

We calculated the dispersion by fitting the experimental data of the V mode with the theoretical model[22], using the contact stiffnesses K_N and G_N as fitting parameters. Since the HR and RH peaks are much smaller and noisier compared to the V mode, we felt that their assignment to the respective dispersion branches needs to be verified. Therefore we only used the V mode in the fitting procedure; small HR and RH peaks were not used. The calculated results are shown in Fig. 2(d) as dashed-dotted curves[25].

The fitted values of the contact stiffnesses are $K_N = 864\,\mathrm{N/m}$, and $G_N = 135\,\mathrm{N/m}$. The corresponding shear stiffness values are $K_S = 684\,\mathrm{N/m}$ and $G_S = 106\,\mathrm{N/m}$. As in prior studies[10], the sphere-substrate contacts are found to be stiffer than the sphere-sphere contacts.

The calculated dispersion curves confirm the assignment of the HR and RH branches. In particular, the calculated HR branch is in good agreement with the measured peaks. The calculated RH branch, on the other hand, is lower than the measured values. As can be seen in Fig 2(e), the RH peak is fairly broad; the discrepancy between the calculated and measured values is within the peak width, although the precision of the peak position measurement that can be assessed from the point-to-point scatter in the data is better than the peak width. The discrepancy can be caused by inaccuracy of the Hertz-Mindlin contact model due to, for example, surface roughness or bending rigidity.

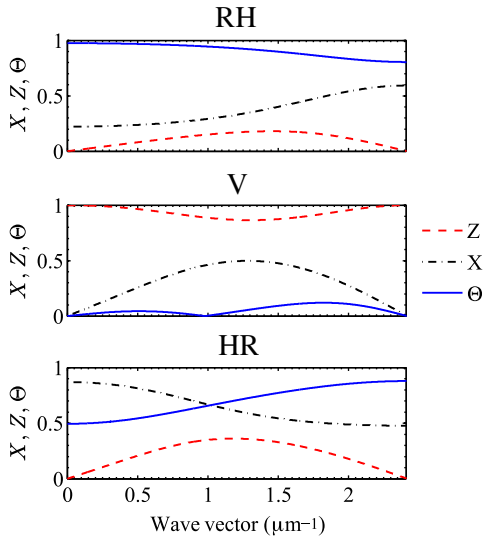

FIG. 3. Relative amplitudes of the displacements and rotations for each contact-based vibrational mode. Z and X denote the amplitudes of the vertical and horizontal displacements of the spheres, while Θ denotes the amplitude of the "rotational displacement", i.e. the product of the rotation angle and the sphere radius. The amplitudes are normalized such that $Z^2 + X^2 + \Theta^2 = 1$.

Figure 3 shows relative contributions of the sphere displacements and rotations for each contact-based mode across the BZ. These modes correspond to the calculated dispersion curves (V, HR, RH) shown in Fig. 2(d). It can be observed that the V mode involves predominantly vertical displacements while the HR and RH modes involve mainly horizontal and rotational motion of the spheres.

We also found indirect evidence of an intersection between the RH and SAW branches in the increased attenuation of the latter. As shown in Fig. 4, the Rayleigh peak width in the Fourier spectrum has a distinct maximum at 235 MHz, while the model predicts the branch crossing at 223 MHz. We note that the presence of such resonant attenuation is consistent with previous observations[10].

Having determined the sphere-substrate contact stiffness, we estimate the width of the SAW bandgap at the BZ boundary. Treating contact springs as a periodic perturbation, we obtained the following expression for the width of the bandgap (see Appendix A),

$$\Delta = \frac{K_N - \chi^2 K_s}{2\omega_R M A_C}, \qquad (1)$$

where A_C is the unit-cell area, ω_R is the (unperturbed) SAW frequency at the BZ boundary, χ is the elipticity of the SAW and M is a constant defined in Ref.[26]. The calculated bandgap width is 1.85 MHz, which is much smaller than the Rayleigh peak width ($\sim$ 16 MHz) and hence cannot be resolved in our measurements; this explains why no bandgap in the SAW dispersion at the BZ boundary is visible in Fig. 2(c).

IV. SPHEROIDAL VIBRATIONAL MODES

A. Sphere-substrate interaction

Turning our attention to the flat branches in the frequency range 600 - 1500 MHz, we attribute them to spheroidal vibrations of the microspheres[27–29], corresponding to four spheroidal modes labeled S_L with angular numbers $L = 0$, 2, 3, 4, and radial number $n = 0$. Table I shows measured and calculated frequencies of these modes averaged over the entire wave vector range. The calculations were done for an isolated sphere on a substrate: we start by calculating the spheroidal mode of a free-sphere[27,28], then account for the contact with the substrate using a perturbation approach[22]. The calculations required the density and acoustic velocities (longitudinal and transverse) of polystyrene, as well as sphere-substrate spring constants K_N and K_S, previously obtained from the dispersion of the vertical contact mode. The density of polystyrene $\rho = 1.04\,\mathrm{g/cm^3}$ was provided by the particle supplier, but the precise values of acoustic velocities were unknown, as for a polymer these may depend on the manufacturing procedure. Therefore, we treated the acoustic velocities as fitting parameters. Our fitted values $c_L = 2323\,\mathrm{m/s}$ and $c_T = 1174\,\mathrm{m/s}$ are in agreement with previously reported values[29].

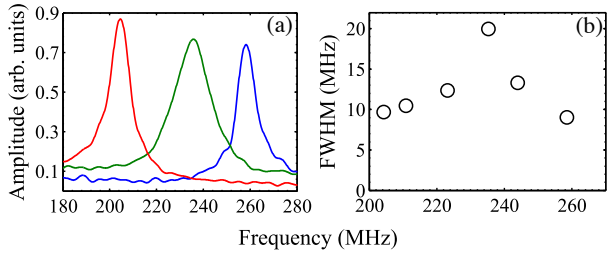

FIG. 4. (a) SAW Fourier peaks in the frequency range 200 - 270 MHz. (b) FWHM of Fourier peaks versus SAW frequency. Peak broadening indicates resonant absorption of SAWs centered at 235 MHZ.

TABLE I. Measured frequencies (in MHz) for observed spheroidal modes and calculated frequencies for an isolated sphere with and without interaction with the substrate.

Mode	Measured freq.	Sphere/substrate	Free-sphere
S_0	1351±4	1351	1347
$S_2^{m=0}$	700 ± 5	689	660
$S_2^{m=1}$	662 ± 2	667	660
S_3	1007 ± 5	1020	983
S_4	1295 ± 4	1305	1262

B. Mode splitting

As shown in Table I, the calculations including the substrate effect are quite close (within 1.5%) to the measured values. Our calculations account for the splitting of the S_2 mode seen at large wave vectors in Fig. 2(c) and shown in detail in Fig. 5. We ascribe this splitting to degeneracy lifting between modes with different azimuthal numbers m due to interaction with the substrate. In the case of free-sphere vibrations, a mode S_L has $2L + 1$ fold degeneracy with an azimuthal number $m = -L, ..., L$ for each degenerate mode. The $n = 0$, S_2 mode of the free-sphere yields 5 degenerate modes with $m = 0, \pm1, \pm2$. For $S_2^{m=0}$, the sphere surface displacement at the contact point is vertical, for $S_2^{m=1}$ (for the purpose of this discussion, we treat $m = \pm1$ modes as a single mode) the displacement is horizontal, and for $S_2^{m=2}$ the displacement at the contact is zero, hence the latter mode is unaffected by the substrate. Since the spheres are optically transparent at the excitation wavelength, spheroidal vibrations can only be excited through the interaction with the substrate. The vertical motion of the substrate surface in the small wave vector limit can only excite the mode $S_2^{m=0}$. The substrate horizontal motion occurs on the time scale λ/c_R, where c_R is the Rayleigh velocity, and is too slow to excite the spheroidal mode at small wave vectors. Therefore, we expect the $S_2^{m=1}$ mode to become observable only at higher wave vectors.

Thus, we identify the main S_2 peak as the $S_2^{m=0}$ mode whereas a smaller lower frequency peak emerging at high wave vectors is ascribed to the $S_2^{m=1}$ mode; as seen in Table I, this assignment agrees with the calculations. Such spheroidal mode splitting due to symmetry breaking by the substrate is not unexpected but has not been previously reported. Indeed, in a more typical measurement with the laser spot centered on an individual particle[30–32]

only the $S_L^{m=0}$ modes can be excited due to symmetry constraints. We expect similar mode splitting to take place for S_3 and S_4 modes; however, the signal from those modes is too weak to detect this phenomenon.

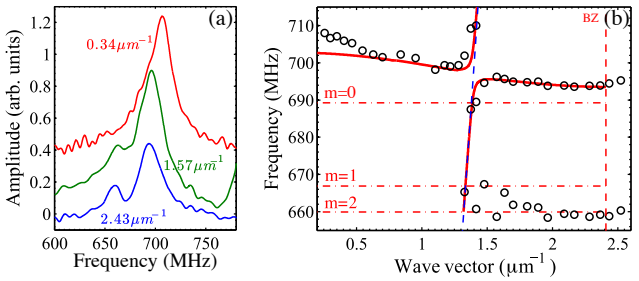

FIG. 5. (a) Representative spectral peaks of the spheroidal mode S_2 for three wave vectors, showing the mode splitting which becomes apparent at large wave vectors. (b) Dispersion of the S_2 mode. Open circles show the measured frequencies. Blue dashed line corresponds to SAW velocity for the substrate, red solid lines corresponds to theoretical calculation for a monolayer of interacting spheres, red dashed lines show calculated frequencies for an isolated sphere.

C. Spheroidal dispersion and interaction with surface Rayleigh waves

Further examination of the $S_2^{m=0}$ mode data shown in Fig. 5(b) reveals a small but appreciable dispersion across the BZ as well as a narrow avoided crossing with the SAW. The dispersion indicates that we are dealing with a collective mode of a microgranular crystal rather than vibrations of individual particles as was assumed in the calculations shown in Table I. The particle-particle interaction can be taken into account using a perturbation approach[22] to obtain an equation relating the frequency ω_1 of the $S_2^{m=0}$ mode to the wave vector q:

$$\omega_1^2 = \omega_0^2 + C_N\frac{K_N}{M_0} + S_N\frac{4G_N}{M_0}\left[2+\cos\left(qD\sqrt{3}/2\right)\right], \quad (2)$$

where ω_0 is the free-sphere frequency, D is the sphere diameter, M_0 is the sphere mass, C_N and S_N are dimensionless constants calculated based on the displacement pattern in the free-sphere mode[22]: $C_N = 3.32$, $S_N = 0.83$. The second term represents the frequency shift due to the sphere-substrate contact while the third describes the dispersion due to the sphere-sphere contact.

Next we modified the effective medium model[7] to describe the interaction of spheroidal vibrations with the SAW in the substrate. This resulted in the following dispersion relation (see Appendix B):

$$(\omega_1^2-\omega^2)\left[\left(2-\frac{\omega^2}{q^2c_{sT}^2}\right)-4\sqrt{1-\frac{\omega^2}{q^2c_{sT}^2}}\sqrt{1-\frac{\omega^2}{q^2c_{sL}^2}}\right] = \frac{K_N\omega^2(\omega_1^2-C_N\frac{K_N}{M_0}-\omega^2)\sqrt{1-\frac{\omega^2}{q^2c_{sL}^2}}}{q^3A_c\rho_s c_{sT}^4}, \quad (3)$$

where $\rho_s = 2.44\,\mathrm{g/cm^3}$, $c_{sT} = 3438\,\mathrm{m/s}$ and $c_{sL} = 5711\,\mathrm{m/s}$ are the density, transverse and longitudinal wave speeds of the substrate, respectively. ω_1 is the spheroidal mode frequency given by Eq. (2). The term in brackets in the left-hand side is the Rayleigh determinant yielding the frequency of the Rayleigh SAW[27]. The right side of Eq. 3 represents the coupling term between the Rayleigh wave and the spheroidal vibrations, effectively determining the width of the avoided crossing.

Figure 5(b) shows the calculated dispersion relation to be in good agreement with the experimental data. This is achieved without any fitting parameters, as the contact spring constants G_N and K_N used in Eqs. (2, 3) were previously determined from the dispersion of the vertical contact mode.

V. CONCLUSIONS

In summary, we studied the linear dynamics of a fully ordered 2D microgranular crystal in the frequency range $0.05 - 2\,\mathrm{GHz}$ and investigated the behavior of three kinds of acoustic modes (contact-based, spheroidal, and Rayleigh) across the entire BZ. A range of previously unexplored phenomena have been revealed, including the dispersion of contact-based and spheroidal modes due to particle-particle interactions, the splitting of a spheroidal resonance due to symmetry breaking by the substrate, and the avoided crossing between a spheroidal mode and the SAW. The experimental results are well described by our analytical models. The two contact stiffnesses obtained from the vertical contact mode dispersion have been shown to describe the observations involving the spheroidal mode dispersion, the Rayleigh-spheroidal avoided crossing, and the absence of the Rayleigh bandgap at the BZ boundary.

We hope this report will stimulate further studies of wave phenomena in ordered microgranular lattices. Nonlinear propagation of high-amplitude waves, 2D lattices with more complicated unit-cells and 3D lattices, dissipation in microgranular systems and thermal transport properties at low temperatures (when low-frequency vibrations control heat transport) present rich opportunities for exploration. The interaction of contact-based and spheroidal modes with SAWs may enable applications in SAW devices and sensors. Another avenue for future research is scaling the particle size down to nanometers, eventually leading to the borderline between granular and molecular crystals.

ACKNOWLEDGMENTS

The work performed at MIT was supported by the U.S. Department of Energy Grant DE-FG02-00ER15087 (experiment) and the National Science Foundation Grant CHE-1111557 (analysis). The work performed at the University of Washington was supported by the National Science Foundation (Grant CMMI-1333858). The work performed at University of Bayreuth was supported by the German Research Foundation SFB840. The work performed at CINVESTAV was partially supported by projects 192 ("Fronteras de la ciencia"), 251882 ("Investigacion Cientifica Basica 2015"), and the fund Conacyt-SENER-Energy-Sustainability (Grant 207450), within the Strategic Project CEMIESol-Cosolpi No. 10 ("Solar Fuels Industrial Proccesses"). A.V-F appreciates support from CINVESTAV and CONACYT through normal, mixed scholarships. C.S. acknowledges support from the Elite Network Bavaria (ENB).

APPENDIX A: BRAGG BAND GAP OF THE RAYLEIGH MODE

In order to find the frequencies of the Rayleigh mode at the BZ boundary, we followed the approach of Ref.[26], Sec. IV. We treat the contact springs as a perturbation increasing the potential energy of the SAW. Since the SAW frequency at the BZ boundary is much larger than the contact resonance frequency, we disregard the center of mass motion of the spheres and assume that the deformation of the contact springs are determined by the SAW surface displacement.

For the even mode (all terms and notations as in Ref.[26]), the perturbation of the potential energy is given by

$$\Delta H_{even} = \frac{1}{2A_c} K_N u^2, \tag{4}$$

where u is the vertical surface displacement amplitude and A_c is the area of the unit cell. For the odd mode, it is given by

$$\Delta H_{odd} = \frac{1}{2A_c} K_S \chi^2 u^2, \tag{5}$$

where χ is the ellipticity of the Rayleigh wave (see Eq. (24) of Ref.[26]). Consequently, the frequencies will be given by

$$\begin{aligned} \omega_{even} &= \omega_R \left(1 + \frac{K_N}{2KA_c}\right), \\ \omega_{odd} &= \omega_R \left(1 + \frac{\chi^2 K_S}{2KA_c}\right), \end{aligned} \tag{6}$$

where ω_R is the Rayleigh frequency and $K = M\omega_R^2$, where M is given by Eq. (23) of Ref.[26]. The bandgap width is given by

$$\Delta = \omega_{even} - \omega_{odd} = \omega_R \frac{K_N - \chi^2 K_S}{2KA_c}. \tag{7}$$

APPENDIX B: SPHEROIDAL-RAYLEIGH WAVE INTERACTION

In order to calculate the spheroidal interaction with the SAW we consider a vertical force F acting on a single sphere at the contact point with the substrate. The equation of motion for the radial displacement ($u_{r,L,m}$) of the spheroidal mode S_L^m at the sphere-substrate contact can be expressed as

$$M_{L,m}\ddot{u}_{r,L,m} = -K_{L,m}u_{r,L,m} - F, \tag{8}$$

where $M_{L,m}$ and $K_{L,m}$ are constants defined in Ref.[22] and related by the expression $K_{L,m} = \omega_0 M_{L,m}$ where ω_0 is the free sphere vibration frequency. The force exerted by the contact spring is

$$F = K_N(u_{r,L,m} + u_z), \tag{9}$$

where u_z is the vertical surface displacement due to elastic waves in the substrate. Applying a Fourier-transform in the time domain we obtain the following relationship for the Fourier-amplitudes of the sphere displacement

$$\begin{aligned} \tilde{u}_{r,L,m} &= \frac{-K_N \tilde{u}_z}{K_{L,m} + K_N - M_{L,m}\omega^2} \\ &= \frac{-K_N \tilde{u}_z}{M_{L,m}(\omega_0^2 + C_N \frac{K_N}{M_0} - \omega^2)}, \end{aligned} \tag{10}$$

where $C_N = M_0/M_{L,m}$ is a dimensionless constant calculated based on the displacement pattern in the free sphere mode[22]. Using Eq. 10 we can determine the vertical force acting on a unit area of the substrate, leading to the following boundary conditions for the SAW at $z = 0$

$$\begin{aligned} \sigma_{zz} &= \frac{K_N(\tilde{u}_r + \tilde{u}_z)}{A_c} = \frac{K_N \tilde{u}_z(\omega_0^2 - \omega^2)}{A_c(\omega_0^2 + C_N \frac{K_N}{M_0} - \omega^2)}, \\ \sigma_{zx} &= 0, \end{aligned} \tag{11}$$

where $A_c = \sqrt{3}D^2/2$ is the area of the unit cell, and M_0 is the mass of the sphere. We follow the standard procedure of deriving the Rayleigh wave dispersion[34], substituting

the stress-free boundary condition by Eq. 11 to obtain the following dispersion relation:

$$\left[\left(2-\frac{\omega^2}{q^2c_{sT}^2}\right)-4\sqrt{1-\frac{\omega^2}{q^2c_{sT}^2}}\sqrt{1-\frac{\omega^2}{q^2c_{sL}^2}}\right]= \frac{K_N\omega^2(\omega_0^2-\omega^2)\sqrt{1-\frac{\omega^2}{q^2c_{sL}^2}}}{q^3A_c\rho_s c_{sT}^4(\omega_0^2+C_N\frac{K_N}{M_0}-\omega^2)}, \tag{12}$$

where ρ_s is the substrate density and c_{sL} and c_{sT} are the longitudinal and transverse wave speeds of the substrate respectively. In the case of interacting spheres, we include the effect of the sphere-sphere interaction by substituting

$$\omega_0^2 \to \omega_0^2 + S_N\frac{4G_N}{M_0}\left[2+\cos qD\sqrt{3}/2\right], \tag{13}$$

into Eq. 12, where S_N is a dimensionless constant defined in Ref.[22]. This leads to the following dispersion relation

$$(\omega_1^2-\omega^2)\left[\left(2-\frac{\omega^2}{q^2c_{sT}^2}\right)-4\sqrt{1-\frac{\omega^2}{q^2c_{sT}^2}}\sqrt{1-\frac{\omega^2}{q^2c_{sL}^2}}\right] = \frac{K_N\omega^2(\omega_1^2-C_N\frac{K_N}{M_0}-\omega^2)\sqrt{1-\frac{\omega^2}{q^2c_{sL}^2}}}{q^3A_c\rho_s c_{sT}^4}, \tag{14}$$

where ω_1 is given by Eq. 2 of the main text. The effective medium approximation we used[7] requires the SAW wavelength to be much greater than the granular lattice constant. In our case, the SAW wavelength amounts to about four lattice constants.

* avegaflick@gmail.com
• maznev@mit.edu

[1] A. N. Lazaridi and V. F. Nesterenko, J. Appl. Mech. Tech. Phys. **26**, 405 (1985).
[2] V. Nesterenko, *Dynamics of heterogeneous materials* (Springer Science and Business Media., 2001).
[3] G. Theocharis, N. Boechler, and C. Daraio, *Nonlinear periodic phononic structures and granular crystals. In Acoustic Metamaterials and Phononic Crystals.* (Springer Berlin Heidelberg, 2013).
[4] V. Laude, *Phononic Crystals: Artificial Crystals for Sonic, Acoustic, and Elastic Waves*, Vol. 26 (Walter Gruyter, Berlin, Germany, 2015).
[5] A. Merkel, V. Tournat, and V. Gusev, Phys. Rev. Lett. **107**, 225502 (2011).
[6] F. Allein, V. Tournat, V. E. Gusev, and G. Theocharis, Extreme Mechanics Letters (2016).
[7] N. Boechler, J. K. Eliason, A. Kumar, A. A. Maznev, K. A. Nelson, and N. Fang, Phys. Rev. Lett. **111**, 036103 (2013).
[8] A. Khanolkar, S. Wallen, M. Abi Ghanem, J. Jenks, N. Vogel, and N. Boechler, App. Phys. Lett. **107**, 071903 (2015).
[9] J. K. Eliason, A. Vega-Flick, M. Hiraiwa, A. Khanolkar, T. Gan, N. Boechler, N. Fang, K. a. Nelson, and A. A. Maznev, App. Phys. Lett. **108**, 061907 (2016).
[10] M. Hiraiwa, M. Abi Ghanem, S. Wallen, A. Khanolkar, A. Maznev, and N. Boechler, Phys. Rev. Lett. **116**, 198001 (2016).
[11] This approach was inspired by earlier experiments on self-assembled colloidal crystals, see Ref.[33].
[12] V. Tournat, I. Pérez-Arjona, A. Merkel, V. Sanchez-Morcillo, and V. Gusev, New J. Phys. **13**, 073042 (2011).
[13] A.-C. Hladky-Hennion, F. Cohen-Tenoudji, A. Devos, and M. de Billy, J. Acoust. Soc. Am. **112**, 850 (2002).
[14] S. P. Wallen, A. A. Maznev, and N. Boechler, Phys. Rev. B **92**, 174303 (2015).
[15] M. Retsch, Z. Zhou, S. Rivera, M. Kappl, X. S. Zhao, U. Jonas, and L. Qin, Macromol. Chem. Phys. **210**, 230 (2009).
[16] H. J. Eichler, P. Gunter, and D. Pohl, *Laser-Induced Dynamic Gratings*, edited by Springer-Verlag (Berlin, 1986).
[17] J. A. Rogers, A. A. Maznev, M. J. Banet, and K. A. Nelson, Annu. Rev. Mater. Sci. **30**, 117 (2000).
[18] A. Vega-Flick, J. K. Eliason, A. A. Maznev, A. Khanolkar, M. A. Abi Ghanem, N. Boechler, J. J. Alvarado-Gil, and K. A. Nelson, Rev. Sci. Instrum. **86**, 123101 (2015).
[19] A. A. Maznev, K. A. Nelson, and J. A. Rogers, Opt. Lett. **23**, 1319 (1998).
[20] G. Goodno, G. Dadusc, and R. Miller, J. Opt. Soc. Am. B **15**, 1791 (1998).
[21] The data points shown in Fig. 2(c,d) where obtained by fitting the Fourier spectra peaks to a Lorentzian function. The window used for the Lorentzian fit was set by cutting the peak at 0.4 of its max value.
[22] A. Vega-Flick, R. A. Duncan, S. P. Wallen, N. Boechler, C. Stelling, M. Retsch, J. J. Alvarado-Gil, K. A. Nelson, and A. A. Maznev, arXiv:1703.04784 [physics.class-ph].
[23] Generally, the lattice of spheres yields 6 contact-based vibrational modes corresponding to 6 degrees of freedom (three translations and three rotations). For a high symmetry direction such as $\Gamma-\mathrm{K}$, there are three modes symmetric with respect with the sagittal plane. We are only interested in these symmetric sagittaly polarized modes[14,22] because antisymmetric ones cannot be excited or probed in our experiment.
[24] K. L. Johnson, *Contact mechanics* (Cambridge university press, 1987).
[25] The best fit dispersion curves shown in Fig. 2(d) were found by minimizing the mean square deviation between the calculated and measured frequencies using the Levenberg-Marquardt algorithm.
[26] A. A. Maznev and A. G. Every, J. App. Phys. **106**, 113531 (2009).
[27] A. C. Eringen and E. S. Suhubi, *Elastodynamics, Volume II Linear Theory* (Academic Press, New York, 1975).
[28] H. Lamb, Proceedings of the London Mathematical Society **1**, 189 (1881).
[29] W. Cheng, J. Wang, U. Jonas, G. Fytas, and N. Stefanou, Nat. Mater. **5**, 830 (2006).

[30] T. Dehoux, T. A. Kelf, M. Tomoda, O. Matsuda, O. B. Wright, K. Ueno, Y. Nishijima, S. Juodkazis, H. Misawa, V. Tournat, and V. E. Gusev, Opt. Lett. **34**, 3740 (2009).
[31] Y. Guillet, B. Audoin, M. Ferrie, and S. Ravaine, Phys. Rev. B **86**, 035456 (2012).
[32] Y. Li, S. Lim, S. C. Ng, Z. K. Wang, M. H. Kuok, E. Vekris, V. Kitaev, F. C. Peiris, and G. A. Ozin, App. Phys. Lett. **88** (2006).
[33] T. Still, W. Cheng, M. Retsch, R. Sainidou, J. Wang, U. Jonas, N. Stefanou, and G. Fytas, Phy. Rev. Lett. **100**, 194301 (2008).
[34] W. M. Ewing and W. S. Jardetzky, *Elastic waves in layered media* (McGraw-Hill, New York, 1957).